Remote Sensing of Environment 232 (2019) 111292

Contents lists available at ScienceDirect

Remote Sensing of Environment

journal homepage: www.elsevier.com/locate/rse

The scattering and re-absorption of red and near-infrared chlorophyll fluorescence in the models Fluspect and SCOPE

Christiaan van der Tol[a,*], Nastassia Vilfan[a], Dimitri Dauwe[b], Maria Pilar Cendrero-Mateo[c,d], Peiqi Yang[a]

[a] University of Twente, Faculty of Geo-Information Science and Earth Observation (ITC), P.O. Box 217, AE Enschede 7500, The Netherlands
[b] Dept. SBG, Centre for Environmental Sciences, Laboratory of Molecular and Physical Plant Physiology, Hasselt University, Diepenbeek, Belgium
[c] Institute of Bio- and Geosciences, Forschungszentrum Jülich GmbH, Jülich, Germany
[d] Image Processing Laboratory (IPL), University of Valencia, Spain

ARTICLE INFO

Edited by Jing M. Chen

Keywords:
Chlorophyll fluorescence
Radiative transfer model
Scattering

ABSTRACT

Scattering and re-absorption have been recognized as relevant aspects for the interpretation of solar induced chlorophyll fluorescence (SIF) in vegetation remote sensing. In an earlier study [Yang and Van der Tol, RSE 215, 97–108, 2018] we addressed the problem of scattering and re-absorption of near-infrared fluorescence in the vegetation canopy. In this study we analyse within-leaf re-absorption of both red and near-infrared fluorescence using the radiative transfer model Fluspect. The leaf scattering determines the ratio of backward to total leaf fluorescence emission $F_b/(F_b + F_f)$. Fluspect reproduces this ratio with an RMSE of less than 0.1, and explains the observed dependence of the spectral shape of this ratio on chlorophyll content and other leaf properties. We further provide a theoretical evaluation of how asymmetric SIF emission affects the SIF of a whole canopy and explain why recent within-canopy scattering models for fluorescence are not valid for red SIF.

1. Introduction

The measurement of solar induced chlorophyll fluorescence (SIF) and reflectance (ρ) of vegetation in the VNIR region of the electromagnetic spectrum is a non-intrusive way to detect aspects of plant structure and functioning (Ustin et al., 2009; Meroni et al., 2009; Ač et al., 2015). The interpretation of SIF requires understanding of three processes that take place in the vegetation sequentially:

1. The absorption of photosynthetically active radiation (PAR) by chlorophylls,
2. The re-emission of a part of the absorbed radiation as fluorescence,
3. The scattering and re-absorption of the emitted fluorescence.

Great progress has been made during the last decades towards understanding these three processes, thus facilitating the exploitation of SIF.

The first process, the absorption of PAR, is evidently the dominant driver of SIF. Recent studies, in which data of satellite derived SIF are analyzed for estimating the gross primary productivity (GPP) of vegetation, all show strong correlations between SIF and absorbed PAR (aPAR) (Joiner et al., 2014; Yoshida et al., 2015; Yang et al., 2015; Guan et al., 2016; Yang et al., 2018a).

The second process is relevant because the efficiency of fluorescence emission depends on the kinetics of photochemistry and other energy dissipation mechanisms. This emission efficiency is therefore a suitable candidate for studying the light reactions of photosynthesis (Zaks et al., 2012). The challenge is that variations in the emission efficiency are usually small, vegetation type specific, and do not always correlate well with photochemical efficiency (Porcar-Castell et al., 2014). One way of estimating the emission efficiency of SIF has been to normalize SIF by estimates of aPAR, thus removing the dominant effect of aPAR. Yang et al. (2015) found that SIF/aPAR correlates positively with GPP/aPAR estimates in field measurements, and Sun et al. (2017) discuss that such correlation of yields may contribute to the close correlation found between satellite SIF and flux tower GPP. However, fluorescence emission efficiency estimated as SIF/aPAR still combines the effects of emission and subsequent scattering (Van der Tol et al., 2016).

Better understanding of the third process, the scattering of fluorescence in the vegetation, is therefore needed. The scattering and re-absorption of fluorescence have been recognized as a potentially important process in satellite SIF studies (Guanter et al., 2014; Guan et al., 2016; Sun et al., 2017). Wavelength dependent scattering of SIF is particularly relevant for the comparison of SIF measurements at

* Corresponding author.
E-mail address: c.vandertol@utwente.nl (C. van der Tol).

https://doi.org/10.1016/j.rse.2019.111292
Received 16 July 2018; Received in revised form 20 June 2019; Accepted 28 June 2019
Available online 11 July 2019

different wavelengths, which is now feasible by exploiting both the O_2A and O_2B atmospheric absorption bands (Cogliati et al., 2015). Romero et al. (2017) modelled the scattering of SIF in the canopy, by considering the absorption, emission and re-emission in a small layer and integrating the fluorescence photon flux over the canopy. They did not differentiate between leaf and canopy radiative transfer, and used isotropic emission by layers in the canopy. Yang and Van der Tol (2018) and Liu et al. (2018) derived analytical solutions for the scattering of fluorescence, and showed that near-infrared fluorescence canopy scattering scales linearly with reflectance and inversely with leaf albedo and canopy light interceptance (the complementary fraction of the light that reaches the soil without interacting with the canopy). This relationship helps to explain the close correlation between near-infrared reflectance and SIF reported earlier (Badgley et al., 2017), and also makes it possible to correct SIF measurements for the illumination and observation geometry.

The relationship does not hold for red fluorescence, and Yang and Van der Tol (2018) show that this is due to within-leaf scattering. The leaf albedo consists of the components of forward (transmittance τ) and backward scattering (reflectance ρ), and likewise, the emission consists of a forward (F_f) and a backward component (F_b). Yang and Van der Tol (2018) demonstrate that if $F_b/F_f \neq \rho/\tau$, then the relationship between canopy reflectance and fluorescence scattering becomes complicated. Both simulations with the radiative transfer model Fluspect (Vilfan et al., 2016) and measurements (Van Wittenberghe et al., 2015) show that this is the case in the red region. This shows that it is important to understand within-leaf scattering in the context of a whole vegetation canopy, and the model Fluspect (Vilfan et al., 2016) embedded in the model 'Soil-Canopy Observation of Photosynthesis and Energy fluxes' (SCOPE) (Van der Tol et al., 2009b) may serve this purpose.

The first objective of this paper is to validate the within-leaf scattering and re-absorption of SIF in the leaf, as simulated with the model Fluspect, against in situ measurements. The second objective is to evaluate the sensitivity of SIF re-absorption at leaf and vegetation canopy level to optical and structural properties. For this purpose the model SCOPE is used, and recent improvements to the canopy scattering routine in this model, RTMf, are presented.

2. Theory

2.1. Fluspect model description

Fluspect quantifies the three processes of absorption, emission and scattering. Here we summarize the implementation of these processes in the model. A full description of Fluspect is given in Vilfan et al. (2016).

2.1.1. Absorption

Fluspect uses an identical scheme as the model PROSPECT (Jacquemoud and Baret, 1990) for radiative transfer of incident radiation on the leaf, based on the plate model of Stokes (1860) extended to a non-integer number of layers N. Absorption is a function of the concentration and specific absorption coefficients of pigments and water. The specific optical coefficients are spectra describing the absorption ' signature' of these constituents. The coefficients for PROSPECT have recently been re-calibrated to in vivo leaf spectroscopy measurements, and an additional pigment, anthocyanins, has been introduced (Féret et al., 2017). We adopted these coefficients in a recent update of Fluspect (Fluspect-CX) in which we also included an absorption coefficient related to the reversible xanthophyll de-epoxidation as a radiative transfer analogy to the photochemical reflectance index (PRI) (Vilfan et al., 2018).

The relation between absorption and concentration is linear in Fluspect. The absorption coefficient K per unit N is:

$$K = \sum_i K_i C_i / N \tag{1}$$

where K_i are the specific absorption coefficients, and C_i are the concentrations of pigments and water.

The fractional absorption by chlorophylls, which is required for estimating the chlorophyll fluorescence emission, is calculated as:

$$k_{Cab,rel} = \frac{K_{Cab} C_{ab}}{KN} \tag{2}$$

This fraction is a spectrum of values [0,1] indicating that the portion of the absorbed light is absorbed by chlorophyll.

Due to 'pigment packaging', the fact that pigments are not homogeneously distributed in the horizontal direction within the leaf, and each observation is a mixture of patches with different concentrations, K_i may decrease with the real C_i (Duysens and Amesz, 1957), causing curvature in the $K_i(C_i)$ relationship. A number of aquatic radiative transfer models take this into account (Behrenfeld et al., 2009; Lutz et al., 1996), but PROSPECT and Fluspect do not. This may cause discrepancies between retrieved and chemically extracted pigment concentrations. In this paper we work with pigment concentrations retrieved from in vivo measurements of reflectance ρ and transmittance τ by inversion of Fluspect rather than destructive measurements, because we expect that these are better indicators of the actual absorption in the leaf structure than the pigment concentrations obtained destructively.

2.1.2. Emission

A fraction of the energy absorbed by chlorophylls (and a larger fraction of the photons) is emitted as fluorescence. This fraction, Φ_F in the literature on active fluorescence, is inversely proportional to the efficiency of all de-excitation pathways combined (Schreiber and Bilger, 1987), which depends on irradiance, the composition of pigments, the saturation of the plastoquinone pool, and the functional cross-section of the antennae (Porcar-Castell et al., 2014). This makes Φ_F leaf specific and dependent on temperature and actual carboxylation rate (Rosema et al., 1998; Van der Tol et al., 2009a, 2014). Fluspect does not explicate the underlying processes and cannot provide the value of Φ_F, which is input to Fluspect.

The wavelength of the emitted fluorescence radiation is described with a probability density function $\phi(\lambda_f)$, the integral of which is unity. It quantifies the probability that a fluorescence photon produced in the pigment bed has a wavelength λ_f [nm]. This function is an input of Fluspect as well, together with other optical coefficients.

The production of fluorescence per unit of radiation incident on a leaf is written as:

$$\mathbf{M_{leaf}}(\lambda_f, \lambda_e) = \Phi_F \phi(\lambda_f) \otimes \left(k_{Cab,rel}(\lambda_e)(1 - R(\lambda_e) - T(\lambda_e))\right)\sigma(\lambda_f, \lambda_e) \tag{3}$$

where $(1 - R(\lambda_e) - T(\lambda_e))$ represents the leaf absorptance, and σ is a matrix of values between zero and one that has been introduced in Fluspect to suppress the few anti-Stokes fluorescence emissions at wavelengths shorter than the excitation light. $\mathbf{M}_{\text{leaf}}$ is a probability density function for the probability that irradiance of wavelength λ_e results in fluorescence irradiance of wavelength λ_f. $\mathbf{M}_{\text{leaf}}$ has the dimensions of the number of fluorescence wavelengths (vertical) and the number of excitation wavelengths (horizontal). The total fluorescence produced in the leaf for any incident light E is:

$$F_{\text{leaf}}(\lambda_f) = \mathbf{M_{leaf}} E(\lambda_e) \tag{4}$$

F_{leaf} can only be equal to the fluorescence flux emanating from the leaf, if the leaf does not absorb in the fluorescence wavelengths. However, this is not the case, and therefore $F_{\text{leaf}} > (F_b + F_f)$, i.e., the sum of the forward (F_f) and backward (F_b) fluxes emanating from the leaf at its boundaries.

2.1.3. Scattering

The scattering and absorption of the fluorescence in the leaf determine forward F_f and backward F_b. Fluspect uses the doubling algorithm to simulate the scattering and absorption in the mesophyll layer

(Hulst, 1957). Before applying the doubling algorithm, the reflectance and transmittance of the whole mesophyll layer are calculated by removing the effect of the refracting leaf-air interfaces. The mesophyll reflectance and transmittance are used to calculate the Kubelka-Munk coefficients. The doubling algorithm consists of the repeated stacking of two identical layers, starting with an initial elementary layer of relative thickness $\varepsilon = 2^{-n}$ and adding an identical layer below. The stacking leads to a layer of thickness $2^n\varepsilon = 1$ after n steps. In Fluspect, $n = 15$. At each step the fluxes at the edges of the combined layer are calculated. The fluorescence emission of the initial layer is calculated similarly to Eq. (3) as:

$$\mathbf{M_f} = \mathbf{M_b} = 0.5\varepsilon\Phi_F\phi(\lambda_f) \otimes k_{\mathrm{Chl}}(\lambda_e)\sigma(\lambda_f, \lambda_e) \quad (5)$$

where k_{Chl} is the Kubelka-Munk absorption coefficient for chlorophyll: the absorption coefficient of chlorophyll for an infinitesimally small layer. It is inferred from K and k_{Chlrel}, which are valid for the whole mesophyll layer rather than a small sub-layer, using Eq. (24) in Vilfan et al. (2016). The initial layer emits fluorescence equally in both directions (up and down), hence the equal sign and the factor 0.5, but $\mathbf{M_f}$ and $\mathbf{M_b}$ start to diverge after the first doubling step. In each step, $\mathbf{M_f}$ and $\mathbf{M_b}$ are amplified by factors that depend on the transmittance and reflectance in both the excitation and emission wavelengths of the combined layer (Appendix C in Vilfan et al. (2016)). Fig. 1 shows the transmittance, reflectance, forward and backward fluorescence of the mesophyll layer normalized by irradiance, at each step of the doubling algorithm for a typical leaf, and the final spectra after adding the refractive leaf-air interfaces. With each step, τ reduces and ρ increases, while F_f and F_b initially increase throughout the spectrum, but later decrease in the red region. Adding the leaf-air interfaces shifts the reflectance spectrum upward, while reducing transmittance and the fluorescence fluxes, except for the F_f above 720 nm, which increases. The upward shift in reflectance is due to the refractive index of the rough leaf surface, an input of Fluspect which has been retrieved from albino leaves by Jacquemoud and Baret (1990).

The output of Fluspect includes ρ, τ and the matrices $\mathbf{M}_b$ and $\mathbf{M}_f$. The fluorescence flux F at either side of the leaf can be calculated afterwards as:

$$F_i = \mathbf{M}_i E \quad (6)$$

were i denotes ' b' or ' f' for backward or forward direction, and E is the irradiance on the leaf (W $m^{-2}\mu m^{-1}$).

It is important to note that ratios of $\mathbf{M}$, such as $\mathbf{M_b}/\mathbf{M_f}$, are only affected by the amplification factors in the doubling algorithm, but they are independent of Φ_F and ϕ. This can be seen from the fact that $\mathbf{M_b}/\mathbf{M_f}$ of the initial thin sublayer was unity. The independence of $\mathbf{M_b}/\mathbf{M_f}$ on Φ_F and ϕ is convenient, because it means that $F_b/(F_f+F_b)$ is a suitable validation target for the radiative transfer of Fluspect.

2.2. Scaling from leaf to canopy

The importance of leaf radiative transfer for top-of-canopy (TOC) SIF becomes clear by considering its relationship with canopy scattering as modelled in SCOPE.

A routine called 'RTMf' of SCOPE uses the output of Fluspect to scale fluorescence from the leaf to the canopy. Leaves are classified according to their optical depth in the canopy and their orientation. For each class, the emission is calculated by multiplying $\mathbf{M_b}$ and $\mathbf{M_f}$ with the irradiance on the leaves following Eq. (6). Not only the irradiance, but also the emission efficiency Φ_F, which is input to Fluspect, is different for each class. To prevent unnecessary repetition of calculations, Fluspect is executed only once using a single value Φ_{Fo} as input. RTMf scales the outputs $\mathbf{M_{bo}}$ and $\mathbf{M_{fo}}$ linear with the actual Φ_F/Φ_{Fo}, which varies per leaf class. The ratio Φ_F/Φ_{Fo} is calculated elsewhere in SCOPE for each leaf class separately, notably with the model of Van der Tol et al. (2014). This model in turn uses the irradiance and micro-meteorological conditions in the leaf boundary layer and leaf temperature as input. These micro-meteorological conditions are estimated with the energy balance routine which simulates non-radiative heat dissipation via phase changes of water (evaporation) and heat exchange with the air via convection and turbulence Van der Tol et al. (2009b).

The spectra of reflectance and SIF radiance at TOC, r and L_F, are further determined by spectrally invariant geometric quantities that describe the scattering in the canopy. Here we summarize RTMf, and present the modifications that have been made to RTMf since the original publication (Van der Tol et al., 2009b).

L_F has contributions from three components:

1. The fluorescence of sunlit leaves in view of the sensor L_s (Eq. (39) in Van der Tol et al. (2009b)),
2. The fluorescence of shaded leaves in view of the sensor L_d (Eq. (41) in Van der Tol et al. (2009b)),
3. The fluorescence that is scattered towards the sensor by leaves and soil in view L_c.

The last component was originally neglected, but it was introduced in SCOPE version 1.60 (2015) because it is not a negligible term (Fig. 2). It comprises the contribution of fluorescence originating from any leaf (irrespective whether it is in view) that reaches the sensor after

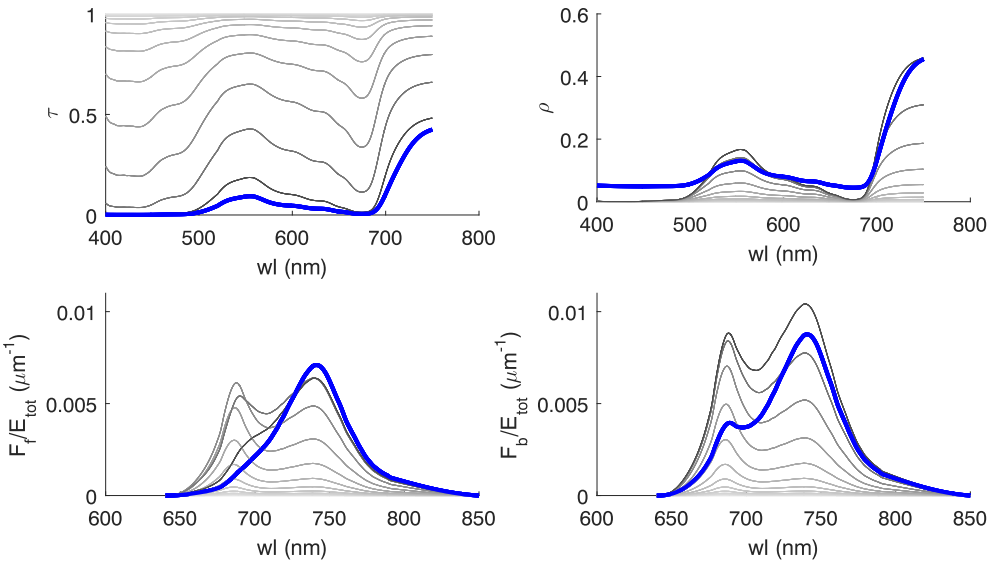

Fig. 1. Transmittance τ, reflectance ρ, forward and F_f backward F_b fluorescence normalized by the spectrally integrated [400–700 nm] irradiance E_{tot} at the 15 doubling steps on a grey scale (light grey: step 1, black: step 15), and after adding the leaf-air interface (blue), for a leaf with a chlorophyll content C_{ab} of 41 $\mu g\ cm^{-2}$ and a mesophyll structure parameter N of 1.67.

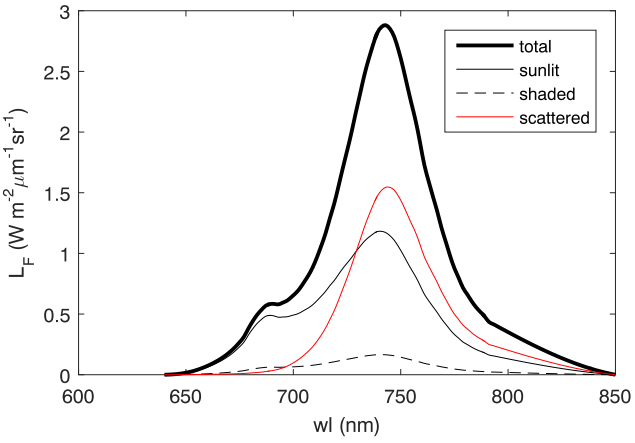

Fig. 2. Typical fluorescence spectra of the contributions of sunlit leaves in view (L_s), shaded leaves in view (L_d), and scattered fluorescence radiance (L_c) to total L_F.

multiple scattering events among leaves and/or soil. It is calculated from the diffuse fluorescence flux inside the canopy, and the last scattering event before escaping the canopy in the direction of the sensor, integrated over the optical depth x in the canopy:

$$\pi L_c = \int_{-1}^{0} P_o(x)(vF^- + v'F^+)dx + P_o(-1)r_s F^-(-1) \tag{7}$$

where v and v' are scattering coefficients for downward and upward diffuse fluxes into observed radiance, r_s is the soil reflectance, $P_o(x)$ the probability to observe a layer at an optical depth x between -1(bottom of canopy) and 0 (TOC), and F^- and F^+ are the downward and upward (diffuse) fluorescence fluxes in the canopy. Note that the contribution of the soil depends on the soil reflectance and the part of the soil that is observed.

The optical depth in SCOPE is discrete, and 60 layers of equal depth are differentiated. Due to the discretization, all integrals in Eqs. (7)–(14) are carried out numerically as summations in SCOPE. The scattering coefficients v and v' are (Yang et al., 2017):

$$v = \int_0^{2\pi}\int_0^{\pi/2}\left(\frac{\rho+\tau}{2}|f_o| + \frac{\rho-\tau}{2}f_o\cos\theta_L\right)p(\theta_L)d\theta_L d\varphi_L, \tag{8}$$

$$v' = \int_0^{2\pi}\int_0^{\pi/2}\left(\frac{\rho+\tau}{2}|f_o| - \frac{\rho-\tau}{2}f_o\cos\theta_L\right)p(\theta_L)d\theta_L d\varphi_L, \tag{9}$$

where f_o is the projected leaf area on the plane perpendicular to the viewing direction. The projection is first calculated per leaf class with geometric relations (Verhoef, 1984), and leaves are classified according to their azimuth angle with respect to the sun φ_L (36 classes), and leaf zenith angle θ_L (13 classes), thus 36×13 classes are differentiated in total. The integration produces a layer-average, weighted with the probabilities that leaf zenith angles occur as defined by a leaf inclination distribution function $p(\theta_L)$ that is input to SCOPE. The coefficients v and v' are spectra with the same dimensions as ρ and τ.

The calculation of the first two contributions to L_F, the emitted fluorescence by sunlit and shaded leaves in view, has not been changed since the first version of SCOPE, except for some re-arrangement to optimize computation speed. The contribution of sunlit leaves in view is (Eq. (39) in Van der Tol et al. (2009b)):

$$\pi L_s = \int_{-1}^{0} (\mathbf{w_F}E_s + \mathbf{v_F}E^- + \mathbf{v'_F}E^+)P_{so}dx \tag{10}$$

and the contribution of shaded leaves in view to observed SIF is (Eq. (41) in Van der Tol et al. (2009b)):

$$\pi L_d = \int_{-1}^{0} (\mathbf{v_F}E^- + \mathbf{v_F}'E^+)(P_o - P_{so})dx \tag{11}$$

where E_s is the direct solar irradiance and E the upward ('+') and downward ('−') diffuse irradiance fluxes in the canopy, all in W $m^{-2}\mu m^{-1}$, P_{so} the probability of observing a sunlit leaf (the bi-directional gap fraction), w_F is the bi-directional fluorescence emission coefficient from solar to observation direction, and $\mathbf{v}_F$ and $\mathbf{v}'_F$ are emission coefficients of fluorescence in observation direction excited by diffuse incident radiation. The emission coefficients are matrices that convert the incident excitation light $E(\lambda_E)$ into a fluorescence spectrum (λ_F) in observation direction. The coefficient $\mathbf{w_F}$ is related to the Fluspect output and the leaf orientations as:

$$\mathbf{w_F} = \int_0^{2\pi}\int_0^{\pi/2}\left(|f_s f_o|\frac{\mathbf{M_b}+\mathbf{M_f}}{2} + f_s f_o\frac{\mathbf{M_b}-\mathbf{M_f}}{2}\right)p(\theta_L)d\theta_L d\varphi_L \tag{12}$$

where f_s is the projected leaf area on the plane perpendicular to the solar beam. The coefficients v_F and $\mathbf{v}_F'$ are also functions of leaf orientation:

$$\mathbf{v_F} = \int_0^{2\pi}\int_0^{\pi/2}\left(|f_o|\frac{\mathbf{M_b}+\mathbf{M_f}}{2} + f_o\frac{\mathbf{M_b}-\mathbf{M_f}}{2}\cos\theta_l\right)p(\theta_L)d\theta_L d\varphi_L \tag{13}$$

$$\mathbf{v_F}' = \int_0^{2\pi}\int_0^{\pi/2}\left(|f_o|\frac{\mathbf{M_b}+\mathbf{M_f}}{2} - f_o\frac{\mathbf{M_b}-\mathbf{M_f}}{2}\cos\theta_l\right)p(\theta_L)d\theta_L d\varphi_L, \tag{14}$$

Note the similarity between the scattering coefficients v and v' (Eqs. (8) and (9)) for incident light and the emission coefficients v_F and v_F' (Eqs. (13) and (14)) for fluorescence, which share the same spectral invariants, notably the projections f_o and f_s. This explains the similarity between reflectance and fluorescence scattering in SCOPE, a feature that has been shown in a more general way by Yang and Van der Tol (2018).

The ' as measured' TOC SIF L_F is the sum of the three components introduced above:

$$L_F = (\pi L_s + \pi L_d + \pi L_c)/\pi \tag{15}$$

Eq. (15) replaces Eq. (43) in Van der Tol et al. (2009b): It includes the additional, previously neglected term πL_c.

With this theoretical frame, we can elucidate the effects of the anisotropic leaf scattering (of incident radiation and emitted fluorescence) on TOC SIF and reflectance due to a bias in the part of the vegetation that is viewed (P_{so} and P_o), and a covariance of the projections of leaves on the solar and viewing plane ($f_o f_s$).

1. The effect of the anisotropy of leaf scattering on canopy scattering of SIF is quantified by second terms on the right hand side of Eqs. (8) to (9), which are proportional to $\rho - \tau$.
2. The effect of the anisotropy of the leaf fluorescence emission on the top-of-canopy fluorescence is quantified by the second terms on the right hand side of Eqs. (12) to (14) which are proportional to $\mathbf{M_b} - \mathbf{M_f}$.

Both terms diminish if leaves were isotropic, resulting in greatly simplified equations, in which a leaf albedo $(\rho + \tau)$ and a single emission of fluorescence suffice. Otherwise, if $\rho/\tau = M_b/M_f$, then the symmetry between the scattering of incident radiation and fluorescence can be exploited to derive simpler relations between TOC SIF and r (Yang and Van der Tol, 2018). In any other case, the relationship between r and SIF must be estimated using knowledge of the asymmetric leaf fluorescence emission.

3. Methodology

3.1. Data

For the purpose of validating the doubling algorithm and its effect on fluorescence scattering, we collected a dataset of 66 leaf spectra of soybean leaves covering a large range of chlorophyll concentrations (https://doi.org/10.17026/dans-xym-hhbq). The field experiment was carried out in Campus Klein Altendorf (CKA), Germany, in August 2015, in collaboration with Forschungszentrum Jülich and the University of Bonn, within the frame of ESA's SoyFLEX field campaign. Measurements were taken on healthy and fully developed leaves of two soybean (*Glycine max* (L.) Merr.) varieties: (1) MinnGold (MG), the yellow, chlorophyll-deficient variant (http://stuparlab.cfans.umn.edu/) and (2) wild-type (WT), green and non-chlorophyll deficient variant. The mutant soybean MG has only 25% of the chlorophyll of the WT variant. Such chlorophyll deficiency changes the properties of the leaves: the leaves are a bright-green to yellow colour, and reflect much more sunlight compared to the WT. Soybean plants grown in the greenhouse were subsequently planted outside on 17 and 19 June 2015.

Leaf level measurements of bidirectional reflectance, transmittance and chlorophyll fluorescence were carried out by means of a spectro-radiometer (FieldSpec 4, ASD Inc.) coupled with a FluoWat leaf clip. The clip has one light entrance at 45°, fitting a light source as well as a short-pass filter (TechSpec, Edmund Optics GmbH, Germany), which blocks the irradiance above 650 nm in order to measure ChlF, and two perpendicular openings for an optical fibre, one at the top and one at the bottom of the clip. The measurement sequence was as follows: a dark current, a measurement of irradiance with a standard reflectance panel slotted into the leaf clip with and without the filter, a sequence of measurements with the leaf (adaxial side up) in the clip with and without the filter, and the fibre in first the top, then the bottom opening (while closing the opposite opening), and an irradiance measurement with and without the filter. Each of these measurements was the average of a batch of five. The procedure to calculate the transmittance of the filter, the calculation of the true from the apparent reflectance and transmittance, and the calculation of the fluorescence spectra are provided in Eqs. (37)–(49) of Vilfan et al. (2016).

The idea was to measure steady state optical properties of leaves in natural conditions at different positions in the canopy. Top and middle layers were illuminated by direct sunlight on clear-sky measurement days. The FluoWat leaf clip is not an integrating sphere, and this poses limitations on the use of the measurements. Leaf reflectance and fluorescence emission are typically not Lambertian, and therefore the measurements may not provide the total emission. Although we verified that $\rho + \tau$ in the near-infrared never exceeded unity, we cannot exclude that the optical properties retrieved from reflectance and transmittance are biased by the observation geometry. The fluorescence observations may be similarly biased. Because specular reflectance is wavelength independent and the refraction is only mildly spectrally dependent, we expect this bias mostly affects the magnitude and less the spectral shape of the signals. In the validation, we did not use the magnitude of the fluorescence, but rather ratios of the fluorescence fluxes from the two sides of the leaf to minimize this problem.

3.2. Validation of the radiative transfer in the leaf

The fluxes F_b and F_f were simulated for all 66 leaves using the PROSPECT-D parameters retrieved per leaf. The unknown spectrally invariant emission efficiency Φ_F was maintained at the default value of 0.01 in all simulations. The spectral shape of the emission ϕ was calibrated to a subset of the leaf samples (Appendix A). The emission spectra used in Fluspect earlier had been obtained from measurements by Franck et al. (2002) in suspension with low chlorophyll content, as described by Miller et al. (2005). The radiative transfer in a suspension differs from that in the leaf structure, which includes the effects of refraction and multiple scattering via cell walls. For this reason it is necessary to calibrate the emission spectrum of chlorophyll in the leaf structure. Indeed, we noticed systematic and obvious discrepancies between the spectral shape of the fluorescence emission simulated with the original spectra of Φ_F for the photosystems I and II as from Franck et al. (2002) and measurements in the original publication of Fluspect (Fig. 8 in Vilfan et al. (2016)) and with spectra published by Magney et al. (2017), with respect to i.e. the sharpness and the exact location of the first peak. The re-calibrated spectrum is included in SCOPE version 1.70, and it improved the match of simulated and measured leaf fluorescence spectra. However, this spectrum of Φ_F should be considered as an intermediate step since our measurements did not allow for a decomposition of the contributions of the two photosystems as in Franck et al. (2002) because we did not have the necessary supporting active fluorescence measurements. For the present analysis, we focus on validation of the ratio of $F_b/(F_f+F_b)$, and for this ratio ϕ is irrelevant.

3.3. Sensitivity analysis at leaf and canopy level

The effects of the parameters of PROSPECT-D on leaf fluorescence were studied by means of a simple one-by-one local sensitivity analysis. Apart from the fluorescence at either side of the leaf, other quantities that are relevant for the interpretation of fluorescence were considered in the sensitivity analysis as well. First, the total initially emitted fluorescence (before re-absorption) in the leaf was calculated with Eq. (4). Second, the probability that generated fluorescence escapes the leaf was calculated as:

$$f_{esc} = \frac{F_b + F_f}{F_{leaf}} \tag{16}$$

Furthermore, the following three ratios for the directionality of the fluorescence from the leaf were computed: $\frac{F_b}{F_b+F_f}$, $\frac{R}{R+T}$ and $\frac{F_b}{R}\frac{R+T}{F_b+F_f}$.

The effects of leaf radiative transfer on the canopy scale were analysed by a similar sensitivity of TOC R, fluorescence radiance L_F, the total emitted fluorescence produced by the whole canopy, and the escape probability to the parameters N, C_{ab}, C_{dm}, C_s. In addition, the sensitivity to leaf area index LAI was analysed. The total fluorescence produced by the whole canopy was calculated by integrating F_{leaf} calculated with Eq. (4), over all leaves:

$$F_{tot} = \int_{-1}^{0}\int_{0}^{2\pi}\int_{0}^{\pi/2} F_{leaf}\, p(\theta_L)\, d\theta_L\, d\varphi_L\, dx \tag{17}$$

4. Results

4.1. Validation of the leaf radiative transfer

Fig. 3 shows reflectance, transmittance and fluorescence spectra, and ratios thereof, for five representative leaves of increasing chlorophyll content (from left to right) covering most of the range, and Fig. 4 scatter plots of simulated versus measured quantities for all 66 leaves. Because Φ_F was maintained constant and the spectra were normalized by the intensity of the (filtered) irradiance, all of the variability in simulated fluorescence among leaves is due to radiative transfer. In that case the model relies on optical properties retrieved from reflectance and transmittance to simulate the fluorescence spectra. The good match between measured and simulated fluorescence demonstrates that most of the variability in the fluorescence can indeed be explained from the optical properties retrieved this way. For example, simulated near-infrared F_b increases with retrieved chlorophyll content (C_{ab}) while red F_f decreases due to re-absorption. Both features appear in the measurements as well. The fifth example leaf has lower near-infrared F than the fourth. This cannot be explained by its high C_{ab}, but rather by strong absorption by other pigments. The relatively low near-infrared F of this leaf is consistent with the lower R and T, and thus higher absorption in

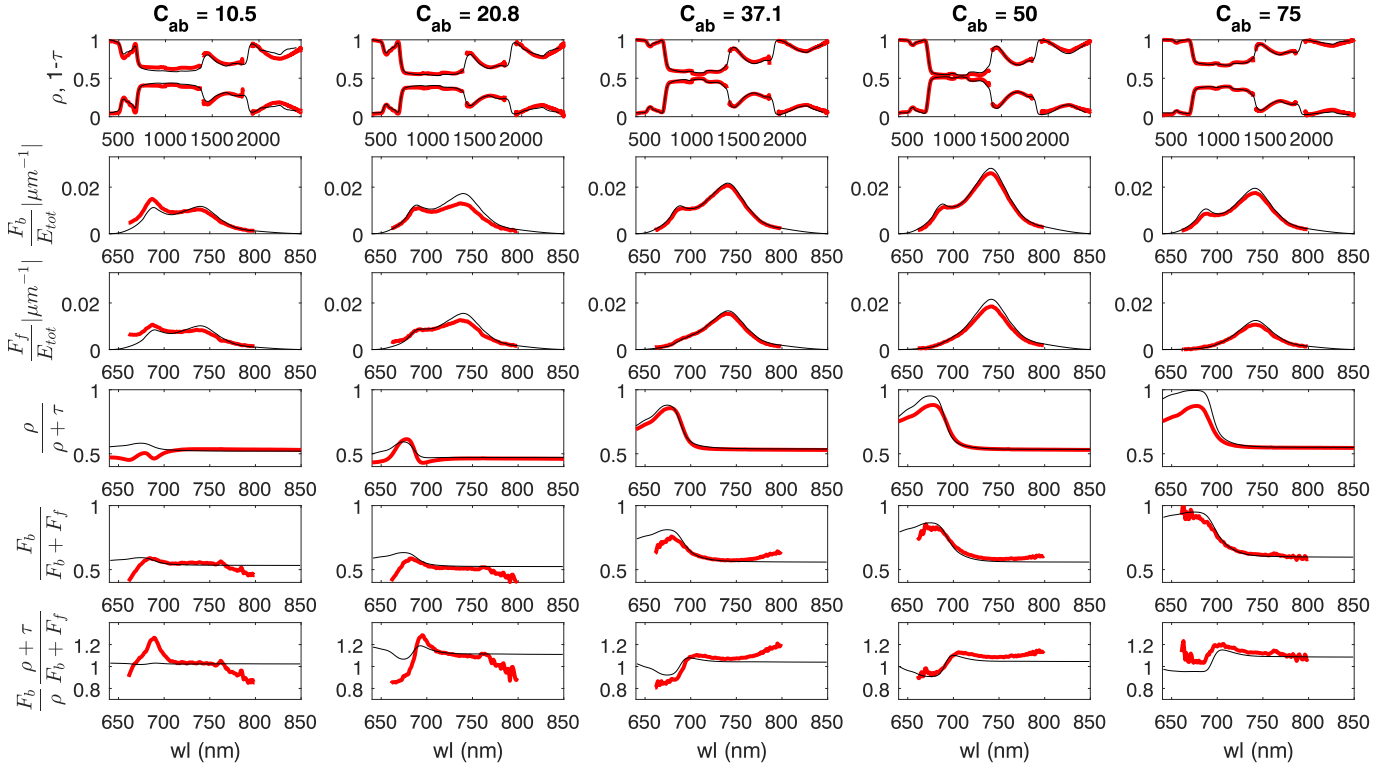

Fig. 3. Measured (bold red) and simulated (black) spectra of reflectance ρ and transmittance τ (top), backward fluorescence F_b (second row), forward fluorescence F_f (third row), the ratio of $\rho/(\rho+\tau)$ (forth row), the ratio of backward to $F_b/(F_b+F_f)$ (fifth row), and the ratio $\frac{F_b}{\rho}\frac{\rho+\tau}{F_b+F_f}$ (bottom row), for two MG leaves (10.6 and 21.8 μg chlorophyll cm^{-2}) and three WT leaves (39.8, 55.3 and 82.5 μg chlorophyll cm^{-2}).

the near-infrared. The model attributes this relatively high absorption to the parameters of dry matter C_{dm} and brown pigments C_s, and via these parameters, reproduces the observed F.

For the purpose of model validation, the ratio $F_b/(F_b+F_f)$ is relevant, because it is independent of potential variations in Φ_F among leaves. This ratio increases with chlorophyll content, and this increase is the strongest in the red region. The fraction of red fluorescence emitted in backward direction increases from 0.6 to more than 0.9 with a chlorophyll content increase from 10.5 to 75 μgcm^{-2}, while the fraction of near-infrared fluorescence emitted in backward direction only increases from 0.5 to 0.6 over this range of chlorophyll content. The ratio $\rho/(\rho+\tau)$ shows a similar pattern: an increase with chlorophyll content, which is the strongest in the red region.

The model cannot explain some observed features in the ratios (bottom two rows in Fig. 3). At the near-infrared tail of the fluorescence spectrum both F_b and F_f are low, and their ratios noisy and prone to

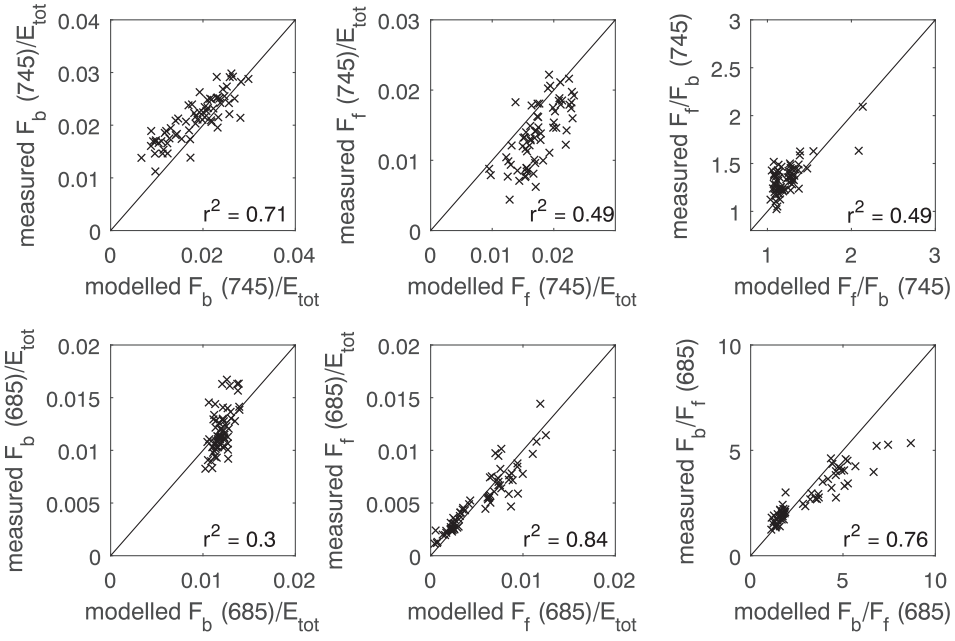

Fig. 4. Measured and Fluspect modelled fluorescence quantities for 66 Soybean leaves of two varieties.

even small offsets in the measurement that may have caused the ratios to decrease in some leaves and increase in others above 760 nm. Furthermore, a ripple in some of the measured ratios at 760 nm indicates that separation of fluorescence from the apparent reflectance was not perfect: A similar albeit small ripple becomes visible in the reflectance and transmittance spectra when zooming in to this region (not shown). The model also does not explain the relatively high red fluorescence at the lowest values of C_{ab} in the measurements. Optical effects due to the presence of the filter may be responsible. We also observe an overestimate in the simulated ratios $\rho/(\rho+\tau)$ and $F_b/(F_b+F_f)$ at low chlorophyll content, which can be explained by the fact that the model simulation of ρ and τ was the least accurate in this spectral region (Fig. 3, upper left panel), possibly due to limitations of the specific absorption spectra. The two outliers in the scatter plots of F_b and Fig. 4 originate from leaves with low C_{ab}, and likewise, the highest values of F_b/F_f that deviate far from the 1:1 line correspond to leaves of low C_{ab}.

Nevertheless, Fig. 4 shows that in this experiment (one species, similar illumination conditions) most of the variability in near-infrared F_b and red F_f among leaves can be explained from radiative transfer alone, with no knowledge on photochemical or non-photochemical quenching. The model performs reasonably in explaining the variabilities in the anisotropic leaf emission of fluorescence.

Fig. 5 quantifies the RMSE and the squared Pearson correlation coefficient for the measured versus the modelled ratios of $\rho/(\rho+\tau)$ and $F_b/(F_b+F_f)$, for all 66 leaves. The RMSE of simulated $\rho/(\rho+\tau)$ decreases with wavelength to values lower than 0.01 in the near-infrared region. The r^2 is above 0.88 at all wavelengths. This indicates that despite discrepancies in ρ and τ in the red region, the model is still able to explain the variations in $\rho/(\rho+\tau)$ caused by differences in chlorophyll content.

Except for the red region, the RMSE of $F_b/(F_b+F_f)$ is higher and the r^2 lower than that of $\rho/(\rho+\tau)$. This can be partly explained by the fact that ρ and τ were used to retrieve pigment contents and thus the model was tuned to these spectra, while the fluorescence data were not used for the retrieval, and partly by the fact that measurements of fluorescence are naturally noisier than those of ρ and τ. The r^2 is high in the red region, where chlorophyll content has the largest influence on $F_b/(F_b+F_f)$, and r^2 decreases with wavelength as $F_b/(F_b+F_f)$ variations among leaves become smaller. Similar to $\rho/(\rho+\tau)$, the RMSE is higher in the red than in the near-infrared.

Yang and Van der Tol (2018) showed the importance of the disparity between the scattering of forward and emitted radiation for the eventual relation between reflectance and fluorescence at the TOC. We are therefore also interested in the ratio $\frac{F_b}{\rho}\frac{\rho+\tau}{F_b+F_f}$ (Fig. 3 bottom). A value of unity for this ratio would simplify the relationship between reflectance and fluorescence at the TOC (Yang and Van der Tol, 2018). At some wavelengths, the ratio is indeed unity, but the measurements also show a peak at 700 nm (>1) and a dip at 680 nm (<1), and Fluspect reproduces this pattern.

The ability of Fluspect to reproduce $\rho/(\rho+\tau)$ and $F_b/(F_b+F_f)$ with an RMSE of less than 0.1 throughout the spectrum, shows that the process descriptions in Fluspect are accurate enough to explain the observed features of fluorescence scattering. This provides confidence in the doubling algorithm and in the following sensitivity analysis of fluorescence scattering.

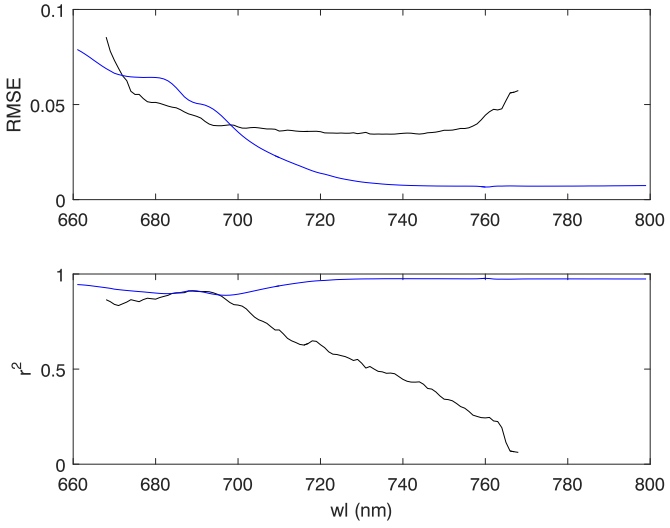

Fig. 5. The RMSE (top) and squared Pearsons correlation coefficient (bottom) of measured versus modelled $\rho/(\rho+\tau)$ (blue) and $F_b/(F_b+F_f)$ (black), for all 66 measured leaves, per wavelength.

4.2. Model sensitivity at the leaf and canopy level

Four parameters had significant effects on the production, the escape probability and/or the directionality of fluorescence, notably the mesophyll structure parameter N the chlorophyll content C_{ab}, the dry matter content C_{dm} and the brown material content C_s. The other model parameters (leaf water content C_w, carotenoid content C_{ca} and anthocyanin content C_{ant}) had only very minor effects on fluorescence, and these are not shown.

Figs. 6 to 9 show simulated fluorescence fluxes produced by chlorophyll within the leaf (Eq. (4)), the fluorescence flux escaping the leaf on either side (backward plus forward) normalized by irradiance, their ratios, and the escape probability.

The mesophyll structure parameter N, a measure for the scattering in the mesophyll, has a negligible effect on the production of fluorescence and the escape probability (Fig. 6a and c), but it has a substantial effect on the directionality of the fluorescence (Fig. 6e). The higher the N, the higher the fluorescence in the backward direction and the lower the fluorescence in the forward direction. This effect is nevertheless smaller than the effect of N on the scattering of incident light: the ratio $\rho/(\rho+\tau)$ varies with N over a wider range than $F_b/(F_b+F_f)$.

The chlorophyll content C_{ab} affects the production (Fig. 7a), the escape probability (Fig. 7c) and the directionality of fluorescence in the red region (Fig. 7e). The production of fluorescence increases with chlorophyll, and this increase is wavelength independent. The increase saturates at higher C_{ab}. The escape probability obviously decreases with C_{ab} in the part of the spectrum that overlaps with the absorption spectrum of chlorophyll. The effect of chlorophyll on the directionality of fluorescence is strong in the red region, but not as strong as its effect on the directionality of the incident light scattering. In the near-infrared, chlorophyll still has a small effect on the directionality of fluorescence, but it has no effect on the directionality of the scattering of incident light.

Dry matter content C_{dm} has neither effect on the production nor the directionality of fluorescence (Fig. 8a and e), but it negatively affects the escape probability in the far-red region (8c). The effect of brown pigments (C_s) is similar to that of C_{dm}, but at different wavelengths (Fig. 9). The absorption by C_s overlaps with that of chlorophyll, and therefore brown pigments compete with chlorophyll for photons. For this reason, C_s affects not only the escape probability, but also the production of fluorescence.

The sensitivity of TOC fluorescence and reflectance to the model parameters is similar to that of the leaf level (Fig. 10). A number of relevant observations can be made:

1. The leaf mesophyll structure parameter N has less effect on fluorescence than on reflectance. While TOC reflectance increases with parameter N, TOC fluorescence shows much lower sensitivity to N. This is due to the lower leaf anisotropy of fluorescence emission than that of incident light scattering, and therefore a lower contribution of the second term of the right hand side in Eqs. (13) and

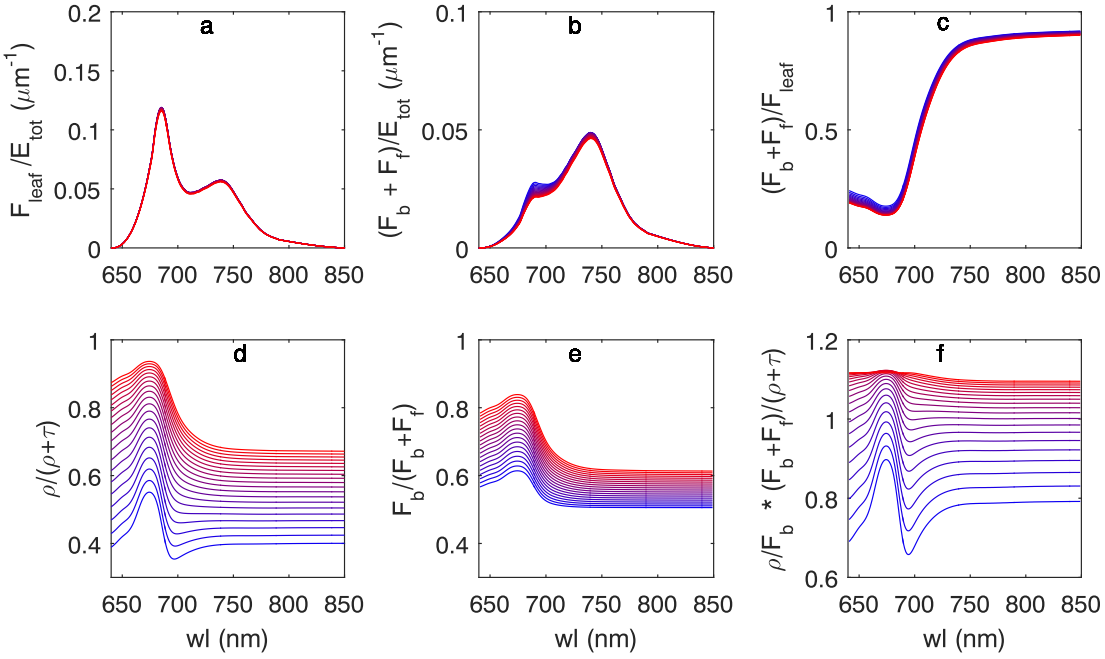

Fig. 6. Fluspect simulated quantities for different values of mesophyll structure N, equally spaced from 1 (blue) to 3 (red). (a) The production of fluorescence by all photosystems, (b) fluorescence emanating from the leaf F_b and F_f, (c) the escape probability of fluorescence from the leaf, (d) the ratio of reflectance over leaf albedo ($\rho/(\rho+\tau)$), the ratio of backward over total fluorescence ($F_b/(F_b+F_f)$, and (f) the ratio $R/F_b(F_b+F_f)/(R+T)$ which quantifies the asymmetry of the direction of scattered light ($\rho/(\rho+\tau)$) and emitted fluorescence ($F_b/(F_b+F_f)$).

(14).

2. The effect of chlorophyll on TOC fluorescence is positive in the near-infrared, and negative in the red (except at C_{ab} lower than 5 μgcm^{-2}). At 750 nm, the effect of C_{ab} on the escape probability is negligible.
3. Dry matter C_{dm} negatively affects the escape probability of near-infrared fluorescence. The magnitude of this effect on fluorescence is similar to the effect of C_{dm} on near-infrared reflectance.
4. Brown material C_s has a significant effect on near-infrared fluorescence, and this effect is stronger than that on reflectance: C_s reduces both the production and the escape probability of fluorescence.
5. Leaf area index LAI affects mostly the production of fluorescence, but it has a marginal effect on the escape probability.
6. The peak ratio of fluorescence, i.e. the ratio of near-infrared to red fluorescence, is mostly determined by C_{ab}, C_{dm} and C_s.
7. The leaf inclination, which determines the projections f_o and f_s, has only a marginal effect on the production of fluorescence, but a strong effect on the observed fluorescence via the escape probability. This results in a higher fluorescence of planophile leaf orientations than erectophile, similar to the higher reflectance of

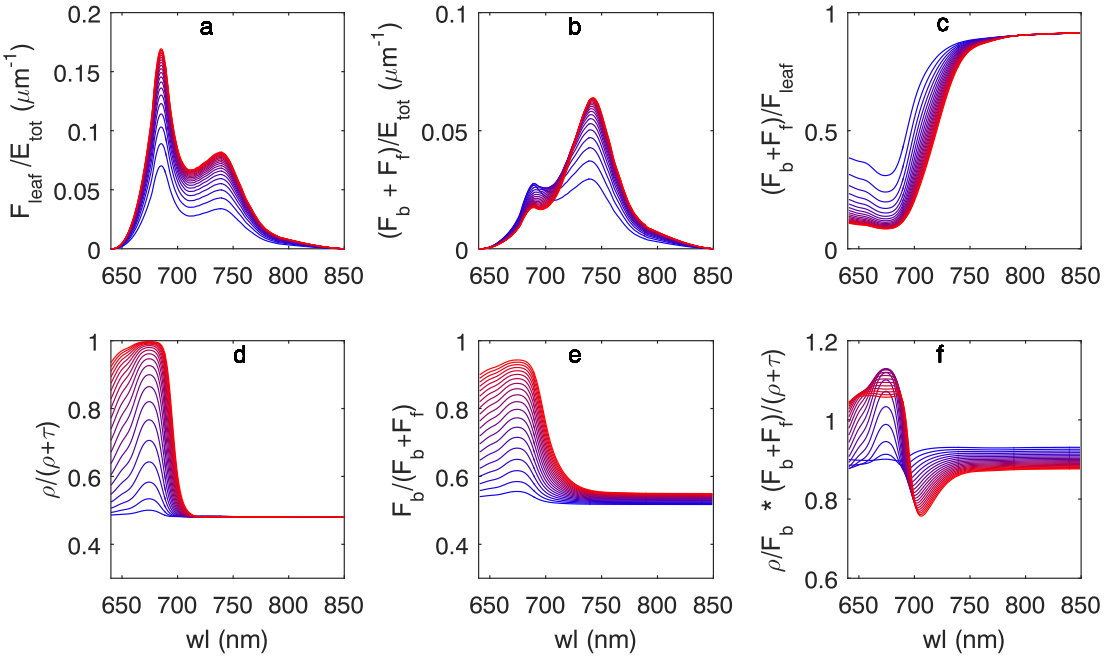

Fig. 7. As in Fig. 6, but each curve represents a value of Chlorophyll concentration C_{ab}, equally spaced from 5 (blue) to 100 (red) $\mu g\ cm^{-2}$).

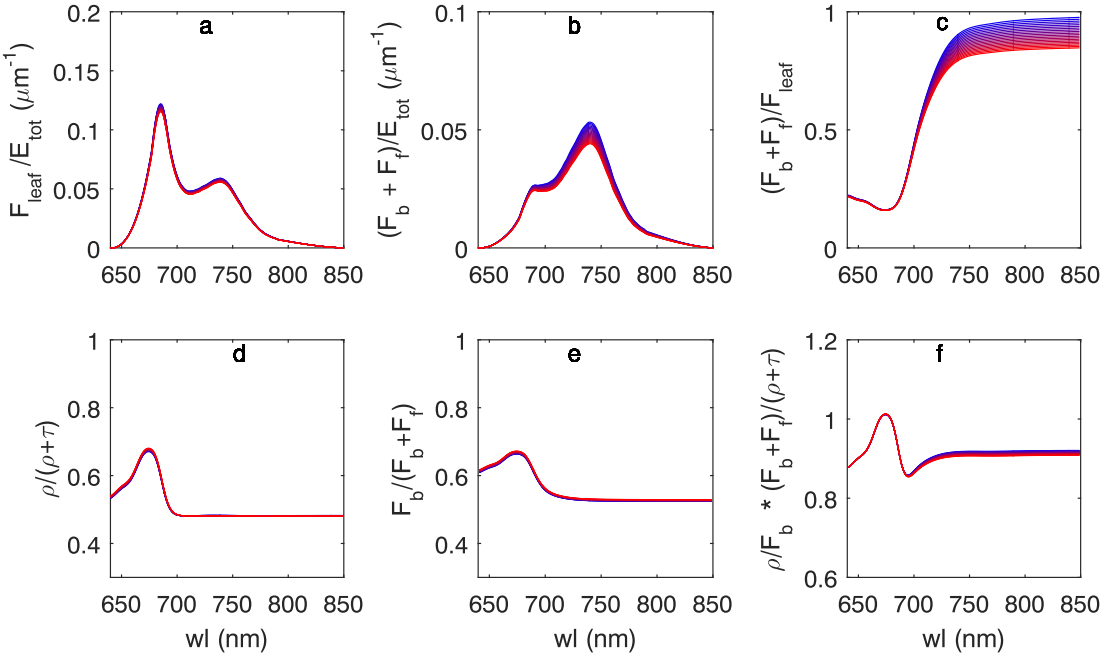

Fig. 8. As in Fig. 6, but each curve represents a value of dry matter content C_{dm}, equally spaced from 0 (blue) to 0.02 (red) mg cm^{-2}).

planophile canopies.

8. The soil reflectance has an effect on SIF that is not negligible (Eq. (7) and Fig. 10). Soil brightness has a small positive effect on the production of fluorescence, and a larger effect on the escape probability of fluorescence from the canopy.

5. Discussion

Our experimental setup allowed for field measurements on intact leaves. The samples from two soybean varieties were dominated by differences in leaf chlorophyll content, while differences in irradiance and leaf physiology were minimized (Sakowska et al., 2018), which suits the purpose of the study. The setup also had several limitations. The FluoWat leaf clip is not an integrating sphere, such that the directional irradiance was not measured. The filter may introduce some additional scattering which cannot be easily quantified. These may explain why we still find a minimal ripple in the reflectance around the Oxygen absorption bands and a rather high fluorescence in the red region for leaves with low chlorophyll content. Furthermore, the filter removes a substantial part of the irradiance, and this affects the fluorescence spectrum since red irradiance is removed from the solar spectrum. However, this does not pose a limitation on the comparison between the model and the measurements. The model uses the measured filtered irradiance spectrum as input, and takes the effect of the wavelength dependent penetration depth of the light into account via the radiative transfer equations.

The models (Fluspect and RTMf) have limitations too. Leaves are much more complex than the model representation in reality. For

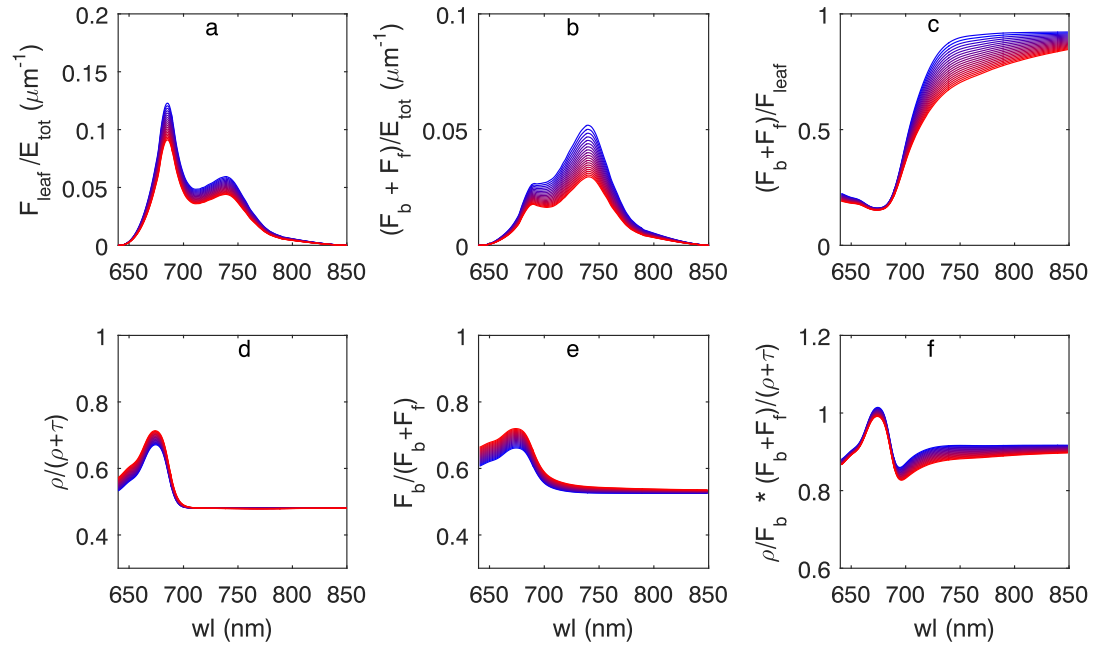

Fig. 9. As in Fig. 6, but each curve represents a value of brown pigment parameter C_s, equally spaced from 1 (blue) to 1.2 (red)).

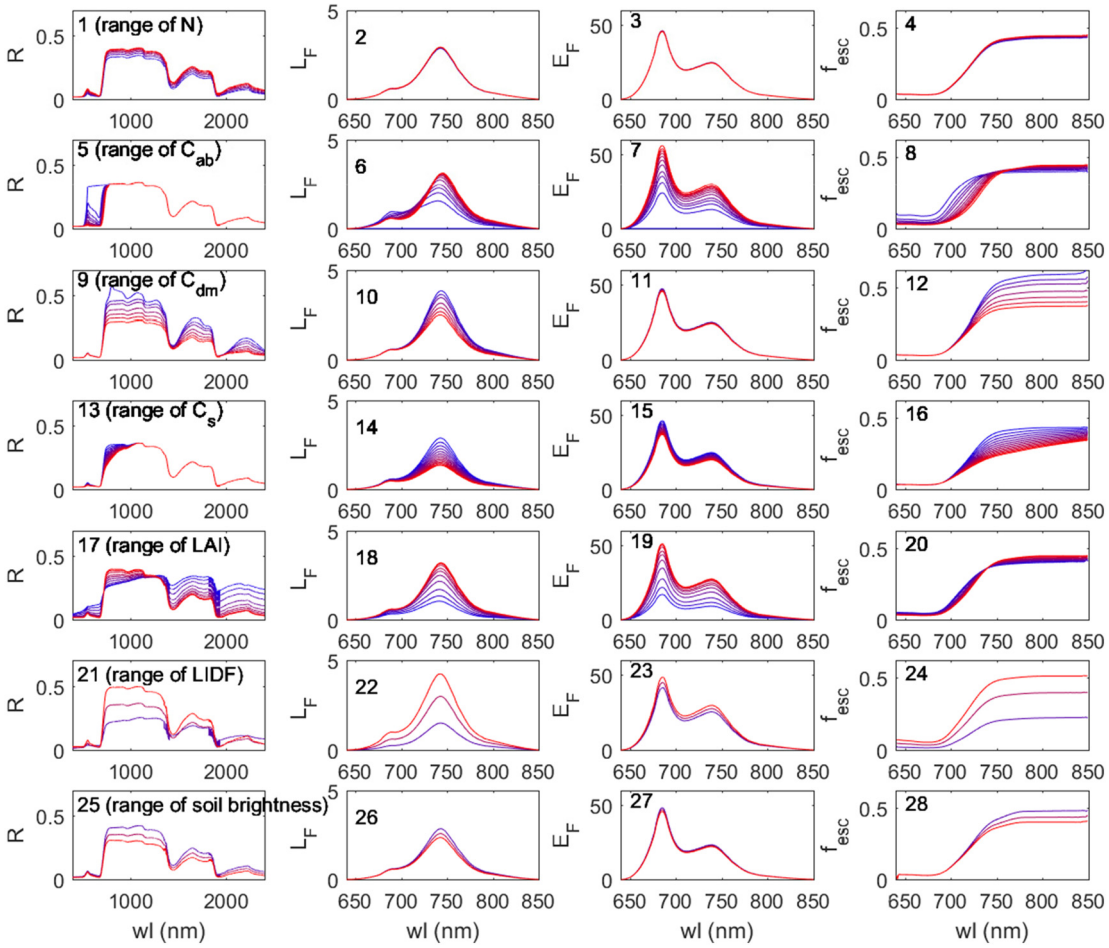

Fig. 10. Reflectance R (1,5,9,13,17,21,25), fluorescence radiance in observation direction L_F (W m^{-2} μmsr^{-1}) (2,6,10,14,18,22,26), total emitted fluorescence in the canopy E_F (W m^{-2} μm) (3,7,11,15,19,23,27), and the escape probability defined as $\pi L_F/F_{prod}{}^{TOC}$ (4,8,12,16,20,24,28), for a range of values of N from 1 to 3 (1–4), C_{ab} from 0 to 100 μgcm^{-2} (5–8), C_{dm} from 0 to 0.02 mgcm^{-2} (9–12), C_s from 0 to 1.2 (13–16), LAI from 0.5 to 7 (17–20), and erectophile (blue), spherical (purple) and planophile leaf inclination distribution (red) (21–24), and soil brightness from nearly black to very bright (25–28). Colour scale is from low (red) to high (blue).

example, leaves have an adaxial and an abaxial side, with different roughness and refractive index. Within the mesophyll layer, a spongy and palisade parenchyma can be differentiated (Terashima and Saeki, 1983). This asymmetrical leaf structure assures optimal light absorption. The palisade is built up with longitudinal shaped cells designed guiding incident light as deep into the leaf as possible. Light that penetrates all the way to the spongy parenchyma is reflected back by circular shaped cells scattering incident light in all directions. While none of these effects is included in Fluspect, they are potentially relevant for remote sensing of plant leaves. A step towards a more realistic model has been made by Stuckens et al. (2009), who included vertical heterogeneity of the mesophyll layer in a radiative transfer model. In view of this complexity, Fluspect is a compromise between realism and applicability in stand-level studies.

Realism versus model applicability is also an issue at the canopy level. SCOPE uses a simple representation of the canopy, while in reality leaf thickness, pigment content and leaf area index may vary among leaves in the canopy depending on their position in terms of optical depth to the top of the canopy. Shaded leaves at the bottom of a canopy are usually thinner and darker (more chlorophyll pigments) compared to sun adapted leaves at the top (Ellsworth and Reich, 1993). While it is possible to use more detailed models, the problem of over-parametrization may occur in case of retrievals.

In this study we have chosen to simplify this scheme and even deliberately maintained the fluorescence emission efficiency Φ_F as a constant. This enables the evaluation of the part of the fluorescence variability that is explained by radiative transfer alone. A remarkably large portion of the variability of fluorescence can be explained this way, and this shows that it is necessary to use fluorescence in combination with traditional reflectance and transmittance measurements to quantify this portion. Obviously, a better fit between model and measurement can be obtained by fitting the Φ_F as an addditional parameter (not shown), but validation of Φ_F retrieved in this way would require measurements of a different type: active measurements of time resolved fluorescence transients or PAM (Porcar-Castell et al., 2014), which we did not carry out. Furthermore, we treated ϕ_f as the sum of the contributions of the two photosystems I and II in the simulations and did not differentate between fluorescence from two photosystems (Franck et al., 2002). Our experimental setup provides no scope for such analysis, but the development of an active system that measures full fluorescence spectra is a promising way forward to obtain the necessary data (Magney et al., 2017). This would be particularly useful in combination with measurements of the reflectance and transmittance spectra.

We further extended the modelling approach to the level of a whole stand, and this fills a knowledge gap between leaf fluorescence studies and the recent studies on fluorescence scattering among leaves in the whole vegetation canopy. This extrapolation of our results on the leaf level to the vegetation canopy scale by means of model simulation is relevant because most applications of SIF focus on understanding the seasonal cycle of satellite derived SIF (Joiner et al., 2014), in which leaf optical properties vary with phenological growth stage. In the analysis

we paid particular attention to the asymmetry of leaf fluorescence emission: The fact that F_b/F_f disagrees to some extend with ρ/τ. This asymmetry poses limitations on the application of recollision theory to explain fluorescence scattering from the reflectance spectrum (Yang and Van der Tol, 2018; Liu et al., 2018). The model explains why these methods do not apply to the red spectral region. Although the projections and gap fractions used in RTMf are calculated with the turbid medium representation of the SCOPE model, the concept has a more general applicability as shown by Yang and Van der Tol (2018), and similar coefficients and relationships may be derived for other radiative transfer models as well. At present, a full radiative transfer model inversion is still needed in order to retrieve vegetation parameters from red fluorescence. Future studies may provide simpler analytical solutions for the within-leaf scattering and re-absorption that circumvent ill-posed and computationally expensive retrievals in analogy those derived to near-infrared fluorescence.

Our sensitivity analyses show that the directionality of the leaf emission is mostly determined by N and C_{ab}, the escape probability by pigments that absorb radiation in the fluorescence emission wavelengths (C_{ab}, C_{dm} and C_s), and the production of fluorescence by LAI, brown pigments C_s and leaf chlorophyll content C_{ab}. Interestingly, both LAI and C_{ab} have relatively minor effects on the escape probability of near-infrared fluorescence, and the reabsorption at this wavelength is mostly caused by C_{dm} and C_s. This may explain the sensitivity of near-infrared fluorescence to forest age. For example, Colombo et al. (2018) showed that stand age affects the ratio of the fluorescence peaks, with relatively higher red fluorescence (as a portion of absorbed PAR) in young forest compared to old forest, which suggests a lower C_{dm} and C_s. The escape probability is mostly affected by the leaf orientation, which determines the exposure of the leaves to solar illumination and observer. This may explain differences in observed SIF among crops with different canopy shape (Yang et al., 2018b) or species communities such as grass or forbs with different leaf orientations (Migliavacca et al., 2017).

6. Conclusion

We made a step towards better understanding the effects of leaf optical properties on fluorescence, in particular it's anisotropic emission (the ratio of backward to forward emitted fluorescence). Leaf optical properties explain a large part of the observed variation of leaf SIF. Their effect can be estimated by making use of concurrent measurements of reflectance and leaf transmittance. By means of model simulation, further we studied the effects of the anisotropy of leaf fluorescence on top-of-canopy SIF, and found that the leaf structure parameter N and leaf chlorophyll content C_{ab} mostly determine the anisotropy, while the escape probability from the canopy is mostly determined by brown pigments and dry matter, and leaf orientations. Although we were not able to validate these findings at the canopy level, we believe this knowledge may nevertheless serve further studies on remote sensing observations of SIF.

Acknowledgments

The fieldwork and research time of Nastassia Vilfan have been funded by the Netherlands Organization for Scientific Research (NWO) in the frame of the Earth and Life Sciences (ALW) division, project ALW-GO/13-32. The fieldwork was further supported by FLEX-EU campaign funded by ESA (contract no. 4000107143/12/NL/FF/lf) and the Forschungszentrum Julich. We are grateful to Luis Alonso for his assistance with using the FluoWat leaf clip. The calibration of the fluorescence emission spectrum was developed during a Short-Term Scientific Mission conducted by D.D. at the University of Twente, supported by the COST Action ES1309/OPTIMISE. P.Y. was supported by a China Scholarship Council grant (201406040058).

Appendix A. Calibration of the emission spectrum

The published version of Fluspect (Fluspect-B) uses two spectra from the literature for ϕ (Franck et al., 2002): ϕ_I and ϕ_{II}, one for each of the photosystems I and II which can be linearly mixed. However, we noted systematic discrepancies in spectral shapes simulated with Fluspect and measured spectra (Fig. A.11). We therefore recalibrated ϕ, but our measurements did not allow for the calibration of two separate spectra for each of the two photosystems. We therefore re-calibrated ϕ using a subset of the *in vivo* leaf measurements, in the following steps:

1. The PROSPECT parameters of chlorophyll (C_{ab}), carotenoid (C_{ca}), dry matter (C_{dm}), anthocyanins (C_{ant}) and leaf water content (C_w), brown pigments (C_s), and the mesophyll thickness parameter (N), were all retrieved by least square regression to measured reflectance (R) and transmittance (T) data of each of the 66 leaves separately, using the optical coefficients of PROSPECT-D.
2. The fluorescence emission spectrum ϕ was calibrated to measured F_b and F_f of a random selection of 8 out of all leaves with a chlorophyll content between 20 and 50 $\mu g\ cm^{-2}$. The PROSPECT-D parameters retrieved in Step 1 were used as model input, and the cost function was a long array consisting of F_b and F_f of all leaves together.

The spectrum ϕ should be defined for the range of 640 to 850 nm, but the calibration of ϕ in Step 2 was limited to the range of 650 to 820 nm due to measurement data quality issues outside this range (filter transmittance and low signal). Rather than calibrating a value of ϕ per nm of wavelength separately, we calibrated a cubic spline function with 85 coefficients (half of the 170 measurement points between 650 and 820 nm) to obtain a smooth curve. For the cubic spline, the Matlab (2015b) function 'csap' was used, and for the minimization of the cost function the 'trust region' method as built in the Matlab (2015b) function 'lsqnonlin', with maximum iterations of 400 and a tolerance for the update step size and cost function value of 10^{-6}. We extrapolated ϕ for both edges, i.e. the ranges 640 to 650 and 820 to 850 nm, by means of third order polynomials forced to zero at both 640 and 850 nm.

The calibrated spectrum of ϕ is shown in Fig. A.11, along with the spectra of ϕ_I and ϕ_{II} originally used in Fluspect. We also show for one leaf, simulations of forward and backward fluorescence using the original spectra and the calibrated spectrum. The calibrated spectrum clearly results in a better match with observations than the original spectra, as shown for one leaf in the example data set in Fig. A.11b and c. The location of the red peak and the tail in the range of 750–800 nm are better represented with the re-calibrated spectrum of ϕ.

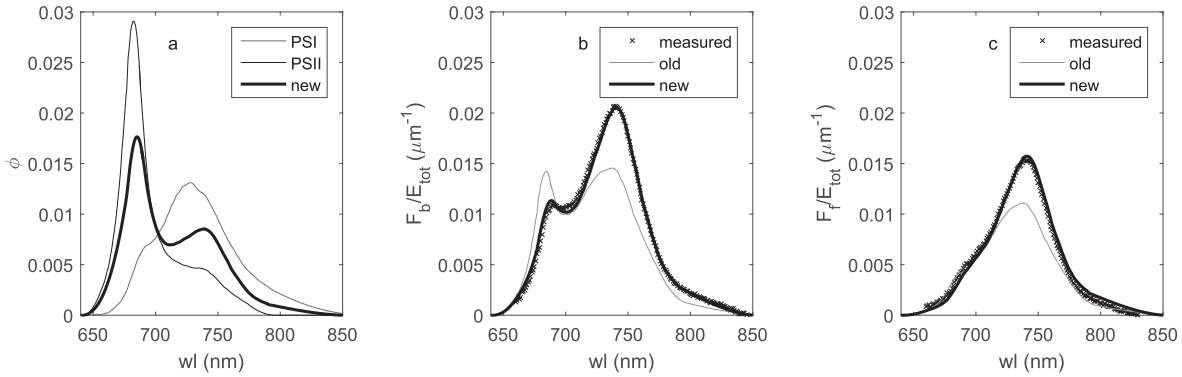

Fig. A.11. Re-calibrated spectrum of ϕ along with the original spectra of ϕ_I and ϕ_{II} (a), and simulation of F_b (b) and F_f normalized by the total PAR irradiance E_{tot} (c) using these spectra for one example leaf with $C_{ab} = 37\mu gcm^{-2}$, $C_{ca} = 7.7\mu gcm^{-2}$ and $N = 1.8$.

References

Ač, A., Malenovský, Z., Olejníčková, J., Gallé, A., Rascher, U., Mohammed, G., 2015. Meta-analysis assessing potential of steady-state chlorophyll fluorescence for remote sensing detection of plant water, temperature and nitrogen stress. Remote Sens. Environ. 168, 420–436.

Badgley, G., Field, C.B., Berry, J.A., 2017. Canopy near-infrared reflectance and terrestrial photosynthesis. Sci. Adv. 3, e1602244.

Behrenfeld, M.J., Westberry, T.K., Boss, E.S., O'Malley, R.T., Siegel, D.A., Wiggert, J.D., Franz, B., McClain, C., Feldman, G., Doney, S.C., et al., 2009. Satellite-detected fluorescence reveals global physiology of ocean phytoplankton. Biogeosciences 6, 779–794.

Cogliati, S., Rossini, M., Julitta, T., Meroni, M., Schickling, A., Burkart, A., Pinto, F., Rascher, U., Colombo, R., 2015. Continuous and long-term measurements of reflectance and sun-induced chlorophyll fluorescence by using novel automated field spectroscopy systems. Remote Sens. Environ. 164, 270–281.

Colombo, R., Celesti, M., Bianchi, R., Campbell, P.K., Cogliati, S., Cook, B.D., Corp, L.A., Damm, A., Domec, J.C., Guanter, L., et al., 2018. Variability of sun-induced chlorophyll fluorescence according to stand age-related processes in a managed loblolly pine forest. Glob. Chang. Biol. 24, 2980–2996.

Duysens, L., Amesz, J., 1957. Fluorescence spectrophotometry of reduced phosphopyridine nucleotide in intact cells in the near-ultraviolet and visible region. Biochim. Biophys. Acta 24, 19–26.

Ellsworth, D., Reich, P., 1993. Canopy structure and vertical patterns of photosynthesis and related leaf traits in a deciduous forest. Oecologia 96, 169–178.

Féret, J.B., Gitelson, A., Noble, S., Jacquemoud, S., 2017. PROSPECT-D: towards modeling leaf optical properties through a complete lifecycle. Remote Sens. Environ. 193, 204–215.

Franck, F., Juneau, P., Popovic, R., 2002. Resolution of the photosystem I and photosystem II contributions to chlorophyll fluorescence of intact leaves at room temperature. Biochim. Biophys. Acta (BBA) - Mol. Basis Dis. - Bioenergetics 1556, 239–246.

Guan, K., Berry, J.A., Zhang, Y., Joiner, J., Guanter, L., Badgley, G., Lobell, D.B., 2016. Improving the monitoring of crop productivity using spaceborne solar-induced fluorescence. Glob. Chang. Biol. 22, 716–726.

Guanter, L., Zhang, Y., Jung, M., Joiner, J., Voigt, M., Berry, J.A., Frankenberg, C., Huete, A.R., Zarco-Tejada, P., Lee, J.E., et al., 2014. Global and time-resolved monitoring of crop photosynthesis with chlorophyll fluorescence. Proc. Natl. Acad. Sci. 111, E1327–E1333.

Hulst, H.C., 1957. Light Scattering by Small Particles. Courier Corporation.

Jacquemoud, S., Baret, F., 1990. PROSPECT: a model of leaf optical properties spectra. Remote Sens. Environ. 34, 75–91.

Joiner, J., Yoshida, Y., Vasilkov, A., Schaefer, K., Jung, M., Guanter, L., Zhang, Y., Garrity, S., Middleton, E., Huemmrich, K., et al., 2014. The seasonal cycle of satellite chlorophyll fluorescence observations and its relationship to vegetation phenology and ecosystem atmosphere carbon exchange. Remote Sens. Environ. 152, 375–391.

Liu, X., Guanter, L., Liu, L., Damm, A., Malenovskỳ, Z., Rascher, U., Peng, D., Du, S., Gastellu-Etchegorry, J.P., 2018. Downscaling of solar-induced chlorophyll fluorescence from canopy level to photosystem level using a random forest model. Remote Sens. Environ.

Lutz, V., Sathyendranath, S., Head, E., 1996. Absorption coefficient of phytoplankton: regional variations in the North Atlantic. Mar. Ecol. Prog. Ser. 197–213.

Magney, T.S., Frankenberg, C., Fisher, J.B., Sun, Y., North, G.B., Davis, T.S., Kornfeld, A., Siebke, K., 2017. Connecting active to passive fluorescence with photosynthesis: a method for evaluating remote sensing measurements of chlfluorescence. New Phytologist 215, 1594–1608.

Meroni, M., Rossini, M., Guanter, L., Alonso, L., Rascher, U., Colombo, R., Moreno, J., 2009. Remote sensing of solar-induced chlorophyll fluorescence: review of methods and applications. Remote Sens. Environ. 113, 2037–2051.

Migliavacca, M., Perez-Priego, O., Rossini, M., El-Madany, T.S., Moreno, G., Van der Tol, C., Rascher, U., Berninger, A., Bessenbacher, V., Burkart, A., et al., 2017. Plant functional traits and canopy structure control the relationship between photosynthetic CO2 uptake and far-red sun-induced fluorescence in a mediterranean grassland under different nutrient availability. New Phytologist 214, 1078–1091.

Miller, J., Berger, M., Goulas, Y., Jacquemond, S., Loius, J., Mohammed, G., Moise, N., Moreno, J., Moya, I., Pedrós, R., 2005. Development of a Vegetation Fluorescence Canopy Model. ESA Scientific and Technical Publications Branch, ESTEC.

Porcar-Castell, A., Tyystjärvi, E., Atherton, J., Van der Tol, C., Flexas, J., Pfündel, E.E., Moreno, J., Frankenberg, C., Berry, J.A., 2014. Linking chlorophyll a fluorescence to photosynthesis for remote sensing applications: mechanisms and challenges. J. Exp. Bot. 65, 4065–4095. https://doi.org/10.1093/jxb/eru191.

Romero, J.M., Cordon, G.B., Lagorio, M.G., 2017. Modeling re-absorption of fluorescence from the leaf to the canopy level. Remote Sens. Environ.

Rosema, A., Snel, J., Zahn, H., Buurmeijer, W., Van Hove, L., 1998. The relation between laser-induced chlorophyll fluorescence and photosynthesis. Remote Sens. Environ. 65, 143–154.

Sakowska, K., Alberti, G., Genesio, L., Peressotti, A., Vedove, G.D., Gianelle, D., Colombo, R., Rodeghiero, M., Panigada, C., Juszczak, R., et al., 2018. Leaf and canopy photosynthesis of a chlorophyll deficient soybean mutant. Plant Cell Environ. 41, 1427–1437.

Schreiber, U., Bilger, W., 1987. Rapid assessment of stress effects on plant leaves by chlorophyll fluorescence measurements. In: Plant response to stress. Springer, pp. 27–53.

Stokes, G.G., 1860. On the intensity of the light reflected from or transmitted through a pile of plates. Proc. R. Soc. Lond. 11, 545–556.

Stuckens, J., Verstraeten, W.W., Delalieux, S., Swennen, R., Coppin, P., 2009. A dorsiventral leaf radiative transfer model: development, validation and improved model inversion techniques. Remote Sens. Environ. 113, 2560–2573.

Sun, Y., Frankenberg, C., Wood, J.D., Schimel, D., Jung, M., Guanter, L., Drewry, D., Verma, M., Porcar-Castell, A., Griffis, T.J., et al., 2017. OCO-2 advances photosynthesis observation from space via solar-induced chlorophyll fluorescence. Science 358.

Terashima, I., Saeki, T., 1983. Light environment within a leaf I. Optical properties of paradermal sections of camellia leaves with special reference to differences in the optical properties of palisade and spongy tissues. Plant Cell Physiol. 24, 1493–1501.

Ustin, S.L., Gitelson, A.A., Jacquemoud, S., Schaepman, M., Asner, G.P., Gamon, J.A., Zarco-Tejada, P., 2009. Retrieval of foliar information about plant pigment systems from high resolution spectroscopy. Remote Sens. Environ. 113, S67–S77.

Van der Tol, C., Berry, J., Campbell, P., Rascher, U., 2014. Models of fluorescence and photosynthesis for interpreting measurements of solar-induced chlorophyll fluorescence. J. Geophys. Res. Biogeo. 119, 2312–2327.

Van der Tol, C., Rossini, M., Cogliati, S., Verhoef, W., Colombo, R., Rascher, U., Mohammed, G., 2016. A model and measurement comparison of diurnal cycles of sun-induced chlorophyll fluorescence of crops. Remote Sens. Environ. 186, 663–677.

Van der Tol, C., Verhoef, W., Rosema, A., 2009a. A model for chlorophyll fluorescence and photosynthesis at leaf scale. Agric. For. Meteorol. 149, 96–105.

Van der Tol, C., Verhoef, W., Timmermans, J., Verhoef, A., Su, Z., 2009b. An integrated model of soil-canopy spectral radiances, photosynthesis, fluorescence, temperature and energy balance. Biogeosciences 6, 3109–3129.

Van Wittenberghe, S., Alonso, L., Verrelst, J., Moreno, J., Samson, R., 2015. Bidirectional sun-induced chlorophyll fluorescence emission is influenced by leaf structure and light scattering properties–a bottom-up approach. Remote Sens. Environ. 158, 169–179.

Verhoef, W., 1984. Light scattering by leaf layers with application to canopy reflectance modeling: the sail model. Remote Sens. Environ. 16, 125–141.

Vilfan, N., Van der Tol, C., Muller, O., Rascher, U., Verhoef, W., 2016. Fluspect-b: a model for leaf fluorescence, reflectance and transmittance spectra. Remote Sens. Environ. 186, 596–615.

Vilfan, N., Van der Tol, C., Yang, P., Wyber, R., Malenovskỳ, Z., Robinson, S.A., Verhoef, W., 2018. Extending fluspect to simulate xanthophyll driven leaf reflectance dynamics. Remote Sens. Environ. 211, 345–356.

Yang, K., Ryu, Y., Dechant, B., Berry, J.A., Hwang, Y., Jiang, C., Kang, M., Kim, J., Kimm, H., Kornfeld, A., et al., 2018a. Sun-induced chlorophyll fluorescence is more strongly related to absorbed light than to photosynthesis at half-hourly resolution in a rice paddy. Remote Sens. Environ. 216, 658–673.

Yang, P., Van der Tol, C., 2018. Linking canopy scattering of far-red sun-induced chlorophyll fluorescence with reflectance. Remote Sens. Environ. 209, 456–467.

Yang, P., Van der Tol, C., Verhoef, W., Damm, A., Schickling, A., Kraska, T., Muller, O., Rascher, U., 2018b. Using reflectance to explain vegetation biochemical and structural effects on sun-induced chlorophyll fluorescence. Remote Sens. Environ. https://doi.org/10.1016/j.rse.2018.11.039. http://www.sciencedirect.com/science/article/pii/S0034425718305480.

Yang, P., Verhoef, W., Van der Tol, C., 2017. The mSCOPE model: a simple adaptation to the scope model to describe reflectance, fluorescence and photosynthesis of vertically heterogeneous canopies. Remote Sens. Environ. 201, 1–11.

Yang, X., Tang, J., Mustard, J.F., Lee, J.E., Rossini, M., Joiner, J., Munger, J.W., Kornfeld, A., Richardson, A.D., 2015. Solar-induced chlorophyll fluorescence that correlates with canopy photosynthesis on diurnal and seasonal scales in a temperate deciduous forest. Geophys. Res. Lett. 42, 2977–2987.

Yoshida, Y., Joiner, J., Tucker, C., Berry, J., Lee, J.E., Walker, G., Reichle, R., Koster, R., Lyapustin, A., Wang, Y., 2015. The 2010 Russian drought impact on satellite measurements of solar-induced chlorophyll fluorescence: insights from modeling and comparisons with parameters derived from satellite reflectances. Remote Sens. Environ. 166, 163–177.

Zaks, J., Amarnath, K., Kramer, D.M., Niyogi, K.K., Fleming, G.R., 2012. A kinetic model of rapidly reversible nonphotochemical quenching. Proc. Natl. Acad. Sci. 109, 15757–15762.